Applied Radiation and Isotopes 146 (2019) 84–89

Contents lists available at ScienceDirect

Applied Radiation and Isotopes

journal homepage: www.elsevier.com/locate/apradiso

Experimental and Monte Carlo characterization of radionuclidic impurities originated from proton irradiation of $[^{18}O]H_2O$ in a modern medical cyclotron

D. Alloni[a,b,*], M. Prata[a,b], B. Smilgys[c]

[a] Applied Nuclear Energy Laboratory (LENA), University of Pavia, via Aselli 41, I-27100, Pavia, Italy
[b] National Institute of Nuclear Physics, INFN, Pavia Unit, Via Bassi 6, I-27100, Pavia, Italy
[c] INSTM, Consorzio Interuniversitario Nazionale per la Scienza e Tecnologia dei Materiali, Unità di Pavia, Via Taramelli 12, I-27100, Pavia, Italy

HIGHLIGHTS

- Fluorine-18 production with cyclotron is described.
- The release of radionuclidic impurities generated by proton irradiation of enriched water as a function of target ageing.
- Gamma spectrometry of irradiated samples.
- Monte Carlo simulation of radionuclide generation inside cyclotron target materials.
- Comparison between Monte Carlo simulation and experimental measurement have been reported.

ARTICLE INFO

Keywords:
Cyclotron
FDG
Radionuclidic impurities
Target ageing
Gamma spectrometry
Monte Carlo simulations

ABSTRACT

In this work we present a characterization of the radionuclidic impurities originated by proton irradiation of enriched water $[^{18}O]H_2O$ in a medical cyclotron through Monte Carlo simulations and experimental measurements. A set of standard samples of enriched water loaded in the cyclotron target cell have been irradiated at 30 μA proton current for 1 h each and, after an appropriate cooling time, measured by HPGe gamma spectrometry. In this way it was possible to study the direct release of radionuclidic impurities from target components as well as the release as a function of target ageing. Previously to experimental measurements, Monte Carlo calculations with the PHITS Code have been carried out to estimate the radionuclides generated within the target components (in particular Havar® foil) with the aim to identify the nuclides expected to be found in the irradiated water due to cell-to-water transmission mechanisms. Comparison between simulations data and experimental measurements by gamma spectrometry showed that only a very small amount of the radionuclides produced in the target window are released in the enriched water through corrosion/erosion effects, while the release decreases with increasing aging of the target.

1. Introduction

Cyclotron-based radionuclide production and chemical synthesis of the marked molecule constitute the two main processes of the production of the most common radionuclides for Positron Emission Tomography (PET) (Alauddin, 2012) such as $[^{18}F]$2-fluoro-2-deoxy-D-glucose $[^{18}F]$FDG. In the production process, (p,n) nuclear reactions induced by 18 MeV proton beam into a target which contains the $[^{18}O]$-enriched water sample give rise to the production of ^{18}F (IAEA, 2009). However, interactions of protons with the materials of the target cell and material activation due to the neutron secondary radiation field produced by the (p,n) reaction (IAEA, 2011), causes the formation and release of radionuclide pollutants during the irradiation process (Bowden et al., 2009; Gillies et al., 2006). The estimation and quantification of these pollutants is an important issue from a radiological point of view because these determine the most efficient way to remove them during $[^{18}F]$FDG synthesis procedures for the final radiopharmaceutical product to be administrated to patients, and, furthermore, to maximize yields during ^{18}F fluorination reactions (Tewson et al., 1988).

* Corresponding author. Applied Nuclear Energy Laboratory, Via Aselli 41, University of Pavia, I-27100, Pavia, Italy.
E-mail address: daniele.alloni@unipv.it (D. Alloni).

https://doi.org/10.1016/j.apradiso.2019.01.026
Received 21 July 2018; Received in revised form 26 January 2019; Accepted 29 January 2019
Available online 31 January 2019
0969-8043/

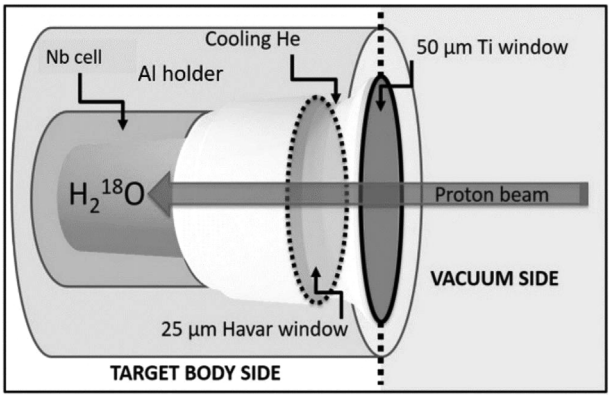

Fig. 1. 3D sketch of the internal target cell.

2. Fluorine-18 production with cyclotron

The cyclotron installed at the Applied Nuclear Energy Laboratory (LENA) of the University of Pavia, is an IBA cyclotron (model Cyclone® 18/9) set up for 18 MeV proton bombardment of a highly ^{18}O-enriched H_2O target (^{18}O > 98.0 Atom %, provided by Huayi Isotopes Co.) with a nominal 30 μA beam current. The ion source generates H^- ions that are subsequently accelerated in the vacuum chamber by a 42 MHz radiofrequency field and maintained in a planar circular orbit by a strong static magnetic field (about 1.5 T at the centre of the machine). When the H^- ion beam reaches the 18 MeV energy value, it is in correspondence of the extraction radius. At this point, the H^- beam traverses a thin carbon foil (stripping foil) undergoing electron stripping and becoming a proton beam, which is then directed to the target due to opposite action of the Lorentz force. Before reaching the enriched volume water, the proton traverses two windows separated by a cooling helium gas flow (see Fig. 1). The first window, made of titanium with a thickness of 50 µm, separates the target body and the flowing helium gas for cooling from the vacuum chamber. The second one, made of Havar®, with a thickness of 25 µm, is, together with niobium cell, in direct contact with the standard 2450 µL loaded volume of enriched water.

3. Formation of radionuclides inside the target cell

Since March 2016, the cyclotron provides two daily productions of ^{18}F delivered to hospital, corresponding to a work load of 10 productions/week, while the remaining time is dedicated to research and machine tests. Every four months a maintenance intervention is scheduled for the cyclotron, in particular, for the more stressed parts such as target components, mechanical and electronic subsystems. During proton bombardment the target cell is the part that is most exposed to the direct proton beam which, with an initial energy of 18 MeV, stops entirely in the loaded enriched water volume, after traversing the target collimator (see Fig. 2) and the two windows. The consequent release of heat in enriched water (about 160 W/cm^2, reaching a temperature of about 240 °C at 20 bar standard irradiation pressure) causes erosive action processes which lead to damage to the niobium cell internal surface, while the windows, in particular the Havar® one, which is in contact with the enriched water, is submitted to direct proton beam interaction as well as corrosive water action. The irradiation-induced water radiolysis pattern responsible for the production of highly reactive species (e.g. radicals, ions, and H_2O_2), makes water an extremely corrosive media with an overall change of water PH value as also outlined in former works (Le Caër, 2011; Buxton, 1987; Spinks and Woods, 1990). The main corrosion damage of cyclotron target Havar window internal surface is caused by the appearance of high local concentrations of these reactive species in the proximity of the internal surface of the window foil. These species diffuse through Havar surface, chemically interacting with the metallic substrate, generating oxidized species of the metals-based Havar alloy which are, subsequently, are partially released into water afterwards.

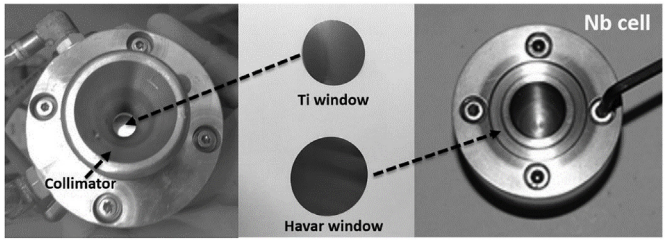

Fig. 2. Target cell disassembled for maintenance. Left: details of the target collimator. Centre: titanium and Havar® windows. Right: niobium cell cavity.

Havar foils are usually used for high pressure target applications because of their high mechanical strength and flexibility (IAEA, 2012), allowing the use of thin beam windows for minimal beam energy attenuation. As a general approach, a target window material has to fulfil a number of mechanical and thermal requirements and also must have high corrosion resistance to irradiated water (Roberts et al., 1995). Upon designing the target for radioisotope production, the selection of proper materials able to meet all of the recalled requirements, is not always possible. Previous works (Skliarova et al., 2015; Wilson et al., 2008) reported that the use of thermally and mechanically suitable substrate materials (e.g. Havar), protected by chemically resistant coating (e.g. Niobium), might be the right technological choice.

From the attenuation/interaction of the proton beam with Havar® window and water, a secondary neutron radiation field (Alloni and Prata, 2017) is also originated by interacting with the target cell and target body materials. Protons and neutrons activation processes yield different radionuclides in cell target and Havar windows which, in turn, are responsible of the enriched-water contamination. In general, the release amount of these pollutants is related to the damage level of the Havar window, and its replacement is the main action to be performed to guarantee and maintain a low contamination level, an improved target efficiency and performance and to prevent, in case of window breakage, undesirable downtime period for restoring the standard irradiation conditions of the cyclotron and its subsystems.

Moreover, an additional water con0074amination radionuclide, that has not been investigated in the present study, is due to the formation of beta-emitters such as tritium via the competing $^{18}O(p,t)^{16}O$ reaction (Schwarz, 2000) Different studies have been published earlier (Ito et al., 2004; Bowden et al., 2009; Remetti et al., 2011; Marshall et al., 2014) which have clearly shown that the tritium activity achieved is related to the on the activity of ^{18}F which, in turns, depends on the proton irradiation conditions (beam current and shape, water pressure, gas flow, water cooling temperature, loaded enriched water volume etc.) and whether any ^3H remains in the target cell from previous irradiations. Moreover, during routinary production of ^{18}F, the irradiation conditions are always maintained as stable as possible in order guarantee the respect of the daily irradiation run time schedule and to fulfil the ^{18}F standard activity requested to be delivered to the hospitals. These stable conditions, together with the irradiation of a new water sample at each irradiation run (water provided by the same supplier), ensures that the tritium production is quite stable and not influenced by the ageing of the target materials.

The presence of these radiochemical pollutants affects the final yield, since they are competitors and/or inhibitors in all its stages of the subsequent FDG synthesis process. The initiators of the development of these interfering species in the target environment can be grouped in different categories as described for example in Remetti et al. (2011).

In this work we focus on the Monte Carlo and experimental characterization of the radionuclidic impurities contained in the proton-irradiated [^{18}O]H_2O originated in the Havar window. Moreover, Monte

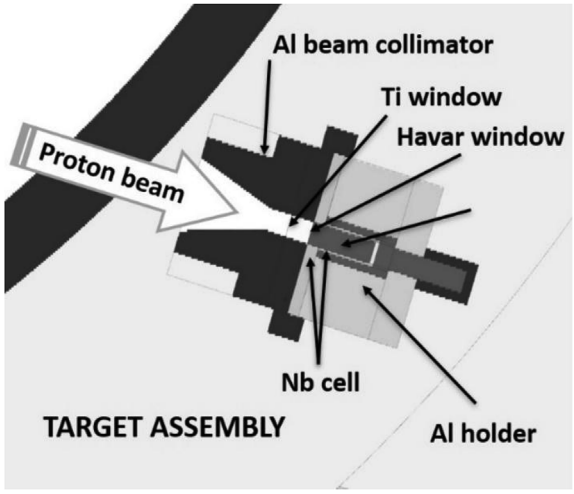

Fig. 3. Model of the whole target built with the PHITS code.

Carlo simulations, as a support to our experimental measurements, allowed for an estimation of the list of the main radionuclides produced in the target Havar window to be compared with experimental measurements.

4. Target modelling and Monte Carlo simulations

All of the Monte Carlo calculations have been performed with the PHITS code, version 3.02 (Particle and Heavy Ion Transport code System), a general purpose particle transport simulation code that can deal with the transport of all particles over wide energy ranges, using several nuclear reaction models and nuclear data libraries (Sato et al., 2013). The PHITS code has been extensively used in the past years and benchmark comparison studies, showing the reliability of PHITS calculation in different areas, have been published in previous works (see for example Sihver et al., 2007; Iwamoto et al., 2017; Sihver et al., 2008).

After particle transport calculation, the PHITS subroutine D-CHAIN estimator allowed to calculate the induced radioactivity after irradiation (EOB – End Of Beam). A detailed model of the whole target has been developed and used (see Fig. 3) as input for the simulations, setting up irradiation parameters to reproduce the standard irradiation conditions (beam energy and shape, target materials, etc).

The target cell (see Fig. 1) is composed by niobium body (inserted in an aluminium holder) and Havar window (thickness 25 μm, density 8.3 g/cm^3; typical composition (Goodfellow® disks): 42.5% Co, 20% Cr, 13% Ni, 2.8% W, 2.4% Mo, 1.6% Mg, 0.2% C, plus residual Fe).

Monte Carlo runs have been performed with a number of starting particles high enough to guarantee a statistical uncertainty less than 5% in the simulation results. Moreover, simulations of proton irradiation have been performed, taking into account the complex and complete geometrical structure and composition of the target.

Transport of primary particles (protons) inside the model have been followed by transport of the secondary particle field such as neutrons and photons. However, some approximations related to the dynamics inside the target cell have been considered. First, recoiling nuclei generated by proton interaction with Havar are not considered in the simulation because of their approximatively zero recoil energy due to the incident proton beam energy of 18 MeV. In the simulations, these nuclei have been considered with zero probability to migrate outside Havar® window and so their Monte Carlo histories have been terminated inside Havar® volume, resulting also in an appreciable reduction of calculation time. Second, water target has been considered in liquid state with its nominal density of 1.111 g/cm^3, therefore proton beam stops entirely inside the water target volume and interaction with internal niobium cell surface can be neglected. The last approximation does not consider target water in vapor state during proton bombardment (i.e low density state), that is a short-time transition condition that appears during long time bombardment. These transition conditions are characterized by water boiling flow and convection mechanisms due to heat transfer. Consequently, a fraction of protons does not stop entirely in the water volume being in a non-homogeneous state and can interact with niobium cell surface generating isotopes such as ^{93m}Mo,^{92m,91m,90}Nb (Ditrói et al., 2009; Lawriniang et al., 2016) that are released into water. However, the concentration of these isotopes must be measured within a couple of days due to their short half-live with respect to the main radionuclides coming from Havar, as the ones reported in this work. As will be discussed later, any contribution of radionuclidic release from niobium is clearly not detectable in the experimental setup presented here, that is through gamma spectrometry after one week of sample cooling. For these reasons, the Havar window under irradiation remains the main source of contaminants release detectable in these measurement conditions.

During the simulation of the primary and secondary radiation transport, the PHITS-coupled subroutine estimator D-Chain has been used to simultaneously calculate the activity of radionuclides inside the Havar® window exposed to the proton beam, as well as its time evolution during, either the bombardment, or after the end of beam. Among the nuclide set obtained by PHITS calculation our attention was mainly focused on to the ones affected by uncertainties not higher than 5% and excluding very short half-life radionuclides. Table 1 reports the results of specific activities of these dominant radionuclides produced in Havar window @ EOB.

Fig. 4 presents the time dependence of the simulated specific activities for the dominant radionuclides from beam start to EOB (60 min). Simulated total activity (TOT ACT) is also reported.

5. Experimental setup and results

The main goal of this study was to estimate radiochemical pollutants generated in the Havar® window through MC simulations and to quantify their release to the enriched water during proton bombardment through gamma spectrometry. Scheduled maintenance program of the ^{18}F target helped us to carry on this study. Every four months, the ^{18}F target is disassembled (see Fig. 2) and the main parts affected by radiation damage and heating stress are replaced with new ones. Within these parts, the target cell is the most important. Before replacement, the new Havar window and the niobium target cell, which are in direct contact with enriched water, have been cleaned with ethanol and ultrasonic bath to remove Havar manufacturing metallic residues which can be released during bombardment and heating, giving further

Table 1
Monte Carlo estimation of the specific activities of the dominant radionuclides in the Havar® window of the target cell @ EOB after 60 min of irradiation @ 30 μA beam current. The third column (i.e. Rate [%]) represents the percentage over the total activity for the specific radionuclide. The total specific activity @ EOB is also reported (this value is bigger with respect to the sum of the activities of the reported radionuclide, since short and very short half-life radionuclides were excluded). Uncertainties for each simulation data on specific activity are less than 5%.

Nuclide	Reaction channel	Specific activity [Bq/cc]	Rate [%]	Half-life [d]
^{51}Cr	^{52}Cr(p,n + p)^{51}Cr	2.6933 × 10^9	0.19	27.7
^{55}Co	^{54}Fe(p,γ)^{55}Co	4.0550 × 10^{11}	28.09	0.72
^{56}Co	^{57}Fe(p,2n)^{56}Co	1.6734 × 10^{11}	11.34	77.27
^{58}Co	Ni(p,x)^{58}Co	5.1319 × 10^{10}	3.55	70.86
^{52}Mn	^{52}Cr(p,n)^{52}Mn	6.1231 × 10^9	0.42	5.59
^{54}Mn	^{54}Cr(p,n)^{54}Mn	4.7152 × 10^9	0.33	312.30
^{183}Re	W(p,x)^{183}Re	1.0456 × 10^8	0.22	70.02
Total activity		1.4438 × 10^{12}	–	–

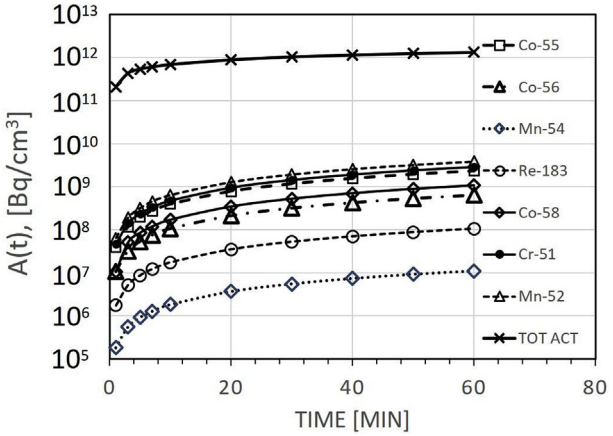

Fig. 4. Buildup for both total specific activity (TOT ACT) in Havar® window and main dominant nuclides contribution which have been calculated with D-Chain subroutine of the PHITS code.

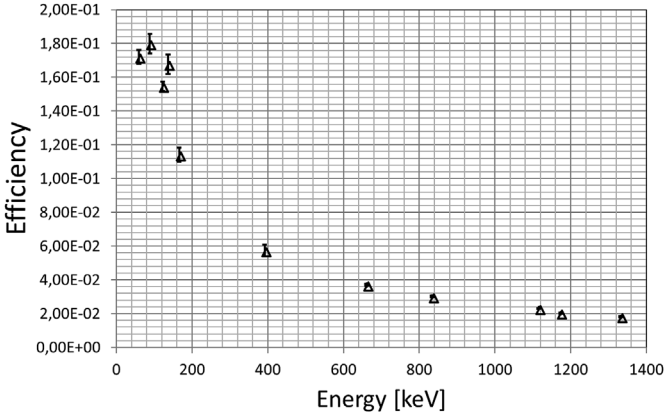

Fig. 5. Detection efficiency curve experimentally determined as a function of energy for the HPGe detector.

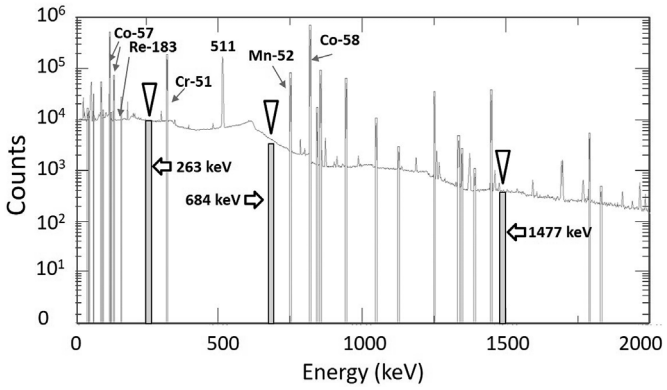

Fig. 6. Spectrum of run#1 sample after maintenance with labelled peaks that indicate the energies of the gammas emitted by radionuclides released from Havar. Marked ROIs (Region of Interest) of the spectrum (grey regions with triangle symbols above) that indicate the energy regions of the gammas emitted by ^{93m}Mo.

contamination and potentially affecting the estimation of pollutants release from the Havar window.

After target maintenance, three samples of irradiated water were produced, transferred to the hot cell and collected in standard glass vials (without further dilution), following this scheme: first sample after maintenance, followed by two sample, each of them separated by ten productions (corresponding temporally to one week).

Each collected sample has been irradiated in the same conditions (2450 μL of enriched water volume @ 20 bar pressure) for 60 min @ 30 μA proton beam current. Table 2 reports the main irradiation parameters for each ^{18}F production.

Irradiated samples have then been collected at room temperature. Gamma spectrometry for radionuclidic content evaluation has been performed on a low-background HPGe coaxial, vertical dip-stick detector (EG&G ORTEC), which has a relative efficiency of 25–30% and a resolution of 1.95 keV FWHM at 1332 keV (with a peak to Compton ratio of 55/1). Background correction has been considered measuring in the same condition a blank sample. The gamma-ray acquisition system consists of MAESTRO® multi-channel Analyzer (MCA) emulation software card, coupled to the detector via electronic modules, all manufactured by EG&G ORTEC. The multi-purpose gamma ray analysis software Gamma Vision® has been used for peaks identification and evaluation. Detector efficiency calibration curve has been obtained using a pointlike standard multigamma source (Am-241, Cd-109, Co-57, Ce-139, Sn-113, Cs-137, Mn-54, Zn-65, Co-60 - product code 12ML01EGMA15, serial number 50131) provided by AREVA NP – LEA, as indicated in Fig. 5. For obtaining this curve, there were performed several measurements to evaluate the efficiency as a function of the geometry, since the vial used for F-18 delivery was not a pointlike source. The reported curve in Fig. 5 is a weighted average of the efficiencies obtained for different positions of the calibration source (i.e. for different distances between the source and the HPGe detector surface).

Fig. 6 reports, as an example, the spectrum of run#1 sample after maintenance analysed in this work. Labelled peaks indicate the energies of the gammas emitted by radionuclides released from Havar, while marked ROIs (Region of Interest) of the spectrum refer, as an example, to the energy regions of the gammas emitted by ^{93m}Mo originating by proton interaction with Niobium and released into the enriched-water volume. As discussed earlier, no evidence for ^{93m}Mo ($t_{1/2}$–6.85 h) peaks is present in the spectrum because one week after EOB, for each analysed sample, basically all the ^{93m}Mo has fully decayed to ^{93}Nb (stable). Tables 3–5 report the data of activities for each sample measurement.

6. Discussion

The comparison of the experimental and simulation results (see Fig. 7) have shown that the amount of nuclides produced in Havar window are several orders of magnitude higher than the ones measured in the irradiated water, indicating that only a very small portion of material is released from the Havar foil to the irradiated enriched-water

Table 2
Main irradiation parameters for the three runs.

Run code	#1	#2	#3
Irradiation date, EOB time	Feb 07/18, 15:30	Feb 14/18, 08:45	Feb 21/18, 13:20
Irradiation length (min)	60	60	60
Beam current (μA)	30	30	30
Cell pressure (Bar)	20	21	20
Measured ^{18}F activity @ EOB (Bq)	8.576×10^{10}	8.456×10^{10}	8.606×10^{10}
Yield (mCi/μAh)	244	240	245

Table 3
Results of gamma spectrometry on sample RUN#1.

Nuclide	Peak energy (keV)	Yield (%)	Efficiency	Uncertainty (%)	Half-life (d)	Activity @ EOB (Bq)	Nuclide % vs. 18F @ EOB
Cr-51	319.89	9.83	7.042×10^{-2}	0.73	27.7	7.21×10^{3}	8.40×10^{-6}
Co-55	1321.37	7.13	1.881×10^{-2}	4.73	0.72	2.84 × 105	3.31×10^{-4}
	1359.79	4.30	1.872×10^{-2}	10.53		2.80 × 105	
Co-56	1238.01	67.65	1.943×10^{-2}	1.32	77.27	6.23×10^{2}	7.11×10^{-7}
	1771.16	15.70	1.340 10^{-2}	3.74		6.10×10^{2}	
Co-57	122.25	85.60	1.615×10^{-1}	0.52	271.73	4.40×10^{2}	5.13×10^{-7}
	136.48	10.60	1.478×10^{-1}	3.41		4.51×10^{2}	
Co-58	810.47	99.45	2.969×10^{-2}	0.27	70.86	5.27×10^{3}	6.14×10^{-6}
Co-60	1174.47	99.86	2.050×10^{-2}	14.41	1925.33	22.60	2.63×10^{-8}
	1332.97	99.98	1.800×10^{-2}	11.04		23.90	
Mn-52	744.23	85.00	3.233×10^{-2}	1.30	5.59	8.45×10^{2}	9.76×10^{-7}
	935.54	93.00	2.578×10^{-3}	1.17		8.37×10^{2}	
Mn-54	835.02	99.98	2.882×10^{-2}	7.74	312.30	37.30	4.35×10^{-8}
Re-183	57.76	43.00	1.702×10^{-1}	12.10	70.02	28.90	3.26×10^{-8}

volume during the bombardment phase following erosion/corrosion effects. Similar results have been found in previous woks using different Monte Carlo codes (Remetti et al., 2011). In general, differences between induced activity calculations with Monte Carlo codes carried out with the same irradiation parameters, depend on several factors among which the compositions of the materials, the nuclear libraries, the detail of the geometry modelling, and the approximations assumed in the physical model to be described.

Moreover, on the experimental side, other works (e.g. Marengo et al., 2008) reported a significant variability of the impurities as measured total activities between different runs. This variability has been attributed to fluctuations in the operating conditions during production (e.g., variations in the integrated charge imposed by production requirements, foil usage, target heating). Despite this variability, some general trends have been drawn from the distribution of the different impurities among the individual components.

The data from gamma ray spectrometry presented in Fig. 7, have shown that this release process tends to reduce with time, irradiation after irradiation, keeping operating conditions during production as stable as possible. This effect can be attributable to an overall reducing effect of the action of reactive chemical species generated in water that react with metals on the surface of the Havar window. This effect involves the formation of a passivation film on Havar surface resulting in a protective action against further oxidative reactions. The formation of a thin passivation layer that covers internal surface of the window acts as a trap reducing the release in subsequent irradiation (target ageing).

Previous works (e.g Skliarova et al., 2015; Wilson et al., 2008) have been also dedicated to the study of the effect of chemically inert coatings with sputtered niobium and niobium oxide on Havar entrance window as a solution to prevent erosion to decrease the amount of ionic contaminants released from Havar. In general, a higher initial release of nuclides can be avoided by carefully cleaning all the spare parts involved in target cell maintenance and keeping all the irradiation condition as stable as possible could reduce the probability to introduce further effects on cell target. As a typical example, the increase of beam current on target to reach irradiation condition efficiency to guarantee high 18F production yield, can induce further release of nuclides due to higher temperature and pressure (e.g. exponential increase of target pressure for increasing beam current) effects on Havar window.

7. Conclusion

In this work a systematic study of the release of nuclides by the target cell material during production of ^{18}F in a medical cyclotron has been presented, showing a decrease of radionuclidic contaminant release as a function of target ageing. The possibility to carry on this study was also due to the presence of a University laboratory equipped with HPGe instrumentation for gamma spectrometry, usually dedicated to the research of environmental radioactivity, which is not the case in most medical centers with a cyclotron. Moreover, detailed studies on cyclotron components behavior, such as target performances under different irradiation conditions, with respect to the standard routine production, were possible, as being the LENA cyclotron not full-time dedicated to the commercial radioisotpes production.

Acknowledgements

The authors are thankful to Mr. Conan Carette, field engineer from IBA (Ion Beam Application,) for the preparation and cleaning of the target components and for taking care of our machine “Luisona” during maintenance visits, and to Dr. Silvana Zanetta for discussions and clarification on chemical issues. This research did not receive any

Table 4
Results of gamma spectrometry on sample RUN#2.

Nuclide	Peak energy (keV)	Yield (%)	Efficiency	Uncertainty (%)	Half-life (d)	Activity @ EOB (Bq)	Nuclide % vs. 18F @ EOB
Cr-51	319.89	9.83	7.042×10^{-2}	0.49	27.7	4.32×10^{3}	5.10×10^{-6}
Co-55	1321.37	7.13	1.881×10^{-2}	9.00	0.72	5.80×10^{4}	6.85×10^{-5}
	1359.79	4.30	1.872×10^{-2}	17.57		6.01×10^{4}	
Co-56	1238.01	67.65	1.943×10^{-2}	2.13	77.27	2.63×10^{2}	3.11×10^{-7}
	1771.16	15.70	1.340 10^{-2}	6.97		2.58×10^{2}	
Co-57	122.25	85.60	1.615×10^{-1}	0.69	271.73	1.97×10^{2}	2.33×10^{-7}
	136.48	10.60	1.478×10^{-1}	3.15		2.00×10^{2}	
Co-58	810.47	99.45	2.969×10^{-2}	0.27	70.86	2.51×10^{3}	2.97×10^{-6}
Co-60	1174,47	99.86	2.050×10^{-2}	37.69	1925.33	12.90	1.52×10^{-8}
	1332.97	99.98	1.800×10^{-2}	13.06		13.20	
Mn-52	744.23	85.00	3.233×10^{-2}	1.44	5.59	4.87×10^{2}	5.66×10^{-7}
	935.54	93.00	2.578×10^{-3}	1.49		4.79×10^{2}	
Mn-54	835.02	99.98	2.882×10^{-2}	13.71	312.30	22.01	2.60×10^{-8}
Re-183	57.76	43.00	1.702×10^{-1}	16.91	70.02	22.80	2.80×10^{-8}

Table 5
Results of gamma spectrometry on sample RUN#3.

Nuclide	Peak energy (keV)	Yield (%)	Efficiency	Uncertainty (%)	Half-life (d)	Activity @ EOB (Bq)	Nuclide % vs. 18F @ EOB
Cr-51	319.89	9.83	7.042×10^{-2}	0.57	27.7	2.33×10^{3}	2.71×10^{-6}
Co-55	1321.37	7.13	1.881×10^{-2}	10.01	0.72	2.33×10^{4}	2.71×10^{-5}
	1359.79	4.30	1.872×10^{-2}	18.24		2.31×10^{4}	
Co-56	1238.01	67.65	1.943×10^{-2}	2.49	77.27	2.34×10^{2}	2.72×10^{-7}
	1771.16	15.70	$1.340\ 10^{-2}$	7.22		2.40×10^{2}	
Co-57	122.25	85.60	1.615×10^{-1}	0.77	271.73	1.62×10^{2}	1.98×10^{-7}
	136.48	10.60	1.478×10^{-1}	3.56		1.70×10^{2}	
Co-58	810.47	99.45	2.969×10^{-2}	0.43	70.86	2.19×10^{3}	2.54×10^{-6}
Co-60	1174,47	99.86	2.050×10^{-2}	41.00	1925.33	31.50	3.66×10^{-8}
	1332.97	99.98	1.800×10^{-2}	7.50		33.00	
Mn-52	744.23	85.00	3.233×10^{-2}	0.93	5.59	1.10×10^{2}	1.28×10^{-7}
	935.54	93.00	2.578×10^{-3}	0.94		1.22×10^{2}	
Mn-54	835.02	99.98	2.882×10^{-2}	11.10	312.30	15.10	1.74×10^{-8}
Re-183	57.76	43.00	1.702×10^{-1}	15.18	70.02	20.00	2.32×10^{-8}

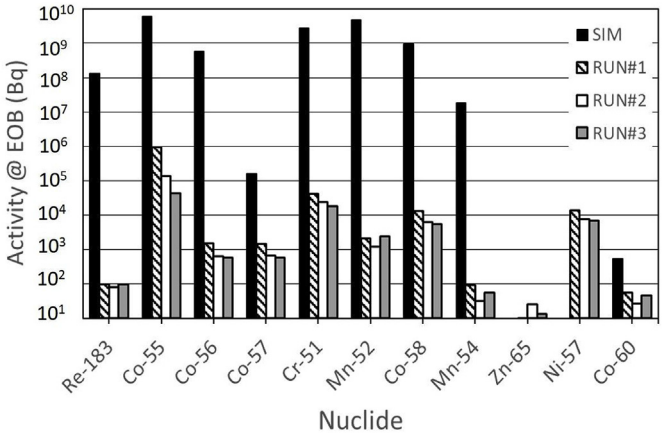

Fig. 7. Distribution of the experimental activity @ EOB for the dominant nuclides compared with simulation results obtained with the PHITS code.

specific grant from funding agencies in the public, commercial, or not-for-profit sectors.

Appendix A. Supplementary data

Supplementary data to this article can be found online at https://doi.org/10.1016/j.apradiso.2019.01.026.

References

Alauddin, M.M., 2012. Positron emission tomography (PET) imaging with 18F-based radiotracers. Amer. J. Nucl. Med. Mol. Imag. 2 (1), 55–76.
Alloni, D., Prata, M., 2017. Characterisation of the secondary neutron field generated by a compact PET cyclotron with MCNP6 and experimental measurements. Appl. Radiat. Isot. 128, 204–209.
Bowden, L., Léon Vintrò, L., Mitchell, P., O'Donnell, R.G., Seymour, A.M., Duffy, G.J., 2009. Radionuclide impurities in proton-irradiated [18O]H2O for the production of 18F: activities and distribution in the [18F]FDG synthesis process. Appl. Radiat. Isot. 67, 248–255.
Buxton, G.V., 1987. In: Farhataziz, Rodgers, M.A.J. (Eds.), Radiation Chemistry. Principles and Applications. Verlag Chemie Publishers, Weinheim, Germany.
Ditrói, F., Hermanne, A., Corniani, E., Takács, S., Tárkányi, F., Csikai, J., Shubin, Y.N., 2009. Investigation of proton induced reactions on niobium at low and medium energies. Nucl. Instrum. Methods Phys. Res. Sect. B Beam Interact. Mater. Atoms 267 (19), 3364–3374.
Gillies, J.M., Najim, N., Zweit, J., 2006. Analysis of metal radioisotope impurities generated in [18O]H2O during the cyclotron production of fluorine-18. Appl. Radiat. Isot. 64, 431–434.
IAEA TECDOC 1211, 2011. Charged Particle Cross-Section Database for Medical Radioisotope Production: Diagnostic Radioisotopes and Monitor Reactions.
IAEA Technical Reports Series No. 468, 2009. Cyclotron Produced Radionuclides: Physical Characteristics and Production Methods.
IAEA Radioisotopes And Radiopharmaceuticals Series, 2012. Cyclotron Produced Radionuclides: Operation and Maintenance of Gas and Liquid Targets. International Atomic Energy Agency, Vienna.
Ito, S., Saze, T., Sakane, H., Ito, S., Ito, S., Nishizawa, K., 2004. Tritium in [18O]water containing [18F]fluoride for [18F]FDG synthesis. Appl. Radiat. Isot. 61 (6), 1179–1183.
Iwamoto, Y., Sato, T., Hashimoto, S., Ogawa, T., Furuta, T., Abe, S., Kai, T., Matsuda, N., Hosoyamada, R., Niita, K., 2017. Benchmark study of the recent version of the PHITS code. J. Nucl. Sci. Technol. 54, 617–635.
Lawriniang, B., Ghosh, R., Badwar, S., Vansola, V., Jyrwa, B., Naik, H., Naik, Y., 2016. Experimental Cross-section Measurement of ^{nat}Nb(p,n)^{93m}Mo reaction up to 20 MeV energy. In: Proceedings of the DAE-BRNS Symposium on Nuclear Physics, vol. 61.
Le Caër, S., 2011. Water radiolysis: influence of oxide surfaces on H2 production under ionizing radiation. Water 3, 235–253.
Marengo, M., Lodi, F., Magi, S., Cicoria, G., Pancaldi, D., Boschi, S., 2008. Assessment of radionuclidic impurities in 2-[18F]fluoro-2-deoxy-D-glucose ([18F]FDG) routine production. Appl. Radiat. Isot. 66, 295–302.
Marshall, C., Talboys, M.A., Bukhari, S., Evans, W.D., 2014. Quantification of the activity of tritium produced during the routine synthesis of (18)F fluorodeoxyglucose for positron emission tomography. J. Radiol. Prot. 34 (2), 435–444.
Remetti, R., Burgio, N.T., Maciocco, L., Arcese, M., Filannino, A., 2011. Monte Carlo simulation and radiometric characterization of proton irradiated [18O]H2O for the treatment of the waste streams originated from [18F]FDG synthesis process. Appl. Radiat. Isot. 69, 1046–1051.
Roberts, A.D., Daniel, L.C., Nickles, R.J., 1995. A high power target for the production of [18F] fluoride. Nucl. Instrum. Methods Phys. Res., Sect. B 99, 797.
Sato, T., Niita, K., Matsuda, N., et al., 2013. Particle and Heavy ion transport code system, PHITS, version 2.52. J. Nucl. Sci. Technol. 50, 913–923.
Schwarz, S.W., 2000. Tritium in [18O]water. In: Proceedings of the Eighth Workshop on Targetry and Target Chemistry, St. Louis, Missouri, US ,23–26 June 1999, pp. 202.
Sihver, L., Mancusi, D., Sato, T., Niita, K., Iwase, H., Iwamoto, Y., Matsuda, N., Nakashima, H., Sakamoto, Y., 2007. Recent developments and benchmarking of the PHITS code. Adv. Space Res. 40, 1320–1331.
Sihver, L., Mancusi, D., Niita, K., Sato, T., Townsend, L., Farmer, C., Pinsky, L., Ferrari, A., Cerutti, F., Gomes, I., 2008. Benchmarking of calculated projectile fragmentation cross-sections using the 3-D, MC codes PHITS, FLUKA, HETC-HEDS, MCNPX_HI and NUCFRG2. Acta Astronaut. 63, 865–877.
Skliarova, A., Renzelli, M., Azzolini, O., de Felicis, D., Bemporad, E., Johnson, R.R., Palmieri, V., 2015. Niobium–niobium oxide multilayered coatings for corrosion protection of proton-irradiated liquid water targets for [18F] production. Thin Solid Films 591, 316–322.
Spinks, J.W.T., Woods, R.J., 1990. An Introduction to Radiation Chemistry, third ed. Wiley-Interscience publication, New York, NY, USA.
Tewson, T.J., Berridge, M.S., Bolomey, L., Gould, K.L., 1988. Routine production of reactive fluorine-18–fluoride salts from an oxygen-18 water target. Nucl. Med. Biol. 15, 499–504.
Wilson, J.S., Avila-Rodriguez, M.A., Johnson, R.R., Zyuzin, A., McQuarrie, S.A., 2008. Niobium sputtered Havar foils for the high-power production of reactive [18F] fluoride by proton irradiation of [18O]H2O targets. Appl. Radiat. Isot. 66, 565.